

UPPSALA
UNIVERSITET



DEPARTMENT OF PHYSICS AND ASTRONOMY
UPPSALA UNIVERSITY

FREIA Report 2018/04
August 2018

Undulator Considerations in the Baseline Design of the MAX IV Soft X-Ray Laser

Alan Mak, Peter Salen, Vitaliy Goryashko

Department of Physics and Astronomy, Uppsala University, Sweden

Department of
Physics and Astronomy
Uppsala University
P.O. Box 516
SE – 751 20 Uppsala
Sweden

Papers in the FREIA Report Series are published on internet in PDF- formats.
Download from <http://uu.diva-portal.org>

Undulator Considerations in the Baseline Design of the MAX IV Soft X-Ray Laser

Alan Mak, Peter Salén, Vitaliy Goryashko

FREIA Laboratory, Uppsala University, SE-75237 Uppsala, Sweden

20th August, 2018

Abstract

We examine the optimal parameter space for an x-ray free-electron laser (FEL) in the operation mode of self-amplified spontaneous emission (SASE). The study focuses on FEL operation with a shorter undulator period and higher undulator strength made available through recent developments in in-vacuum, cryogenic and superconducting undulators. We survey the progress on short-period undulator technologies and compute the FEL output characteristics versus the undulator parameters. We perform the study on a case of the planned soft-x-ray FEL at the MAX IV Laboratory in Sweden. An extension of the SASE mode into the harmonic lasing self-seeded mode is also analysed.

1 Introduction

The x-ray free-electron laser (FEL) is a coherent and tunable light source which offers a spatial resolution at the ångström scale and a temporal resolution at the femto- and attosecond scales. It delivers the highest peak brilliance amongst laboratory x-ray sources today, outperforming even the synchrotron by five to ten orders of magnitude (see Fig. 1).

Thanks to these superb optical properties, the x-ray FEL has opened up many new frontiers in solid-state physics [1], photochemistry [2], structural biology [3] and other research disciplines. In the spectral region of soft x-ray, the FEL has proven useful for coherent diffraction imaging and time-resolved x-ray spectroscopy. The former is performed routinely at the FLASH [4, 5] and FERMI [6, 7] facilities. The latter has been applied to the studies of, for instance, artificial photosynthesis [8] and correlations between valence electrons and holes [9]. The increasing number of scientific applications and the growing demand for beam time motivate the development of new FEL facilities.

However, the x-ray FEL facilities in operation today are generally long, and are not readily affordable for all laboratories. A new direction for research and development, therefore, is to make the FEL more compact while seeking a higher brilliance [10]. This is also the primary objective of the international project “Compact Light” [11], funded by the European Union’s Horizon 2020 Research and Innovation Programme.

One approach to a more compact FEL is to take advantage of the advancements [12, 13] in cryogenic, superconducting and in-vacuum undulator technologies, so as to reduce the undulator length required for reaching a high brilliance. In this article, we study this approach by means of analytical calculations and numerical simulations, on a case of the Soft X-Ray Laser (SXL) project [14] at the MAX IV Laboratory in Sweden.

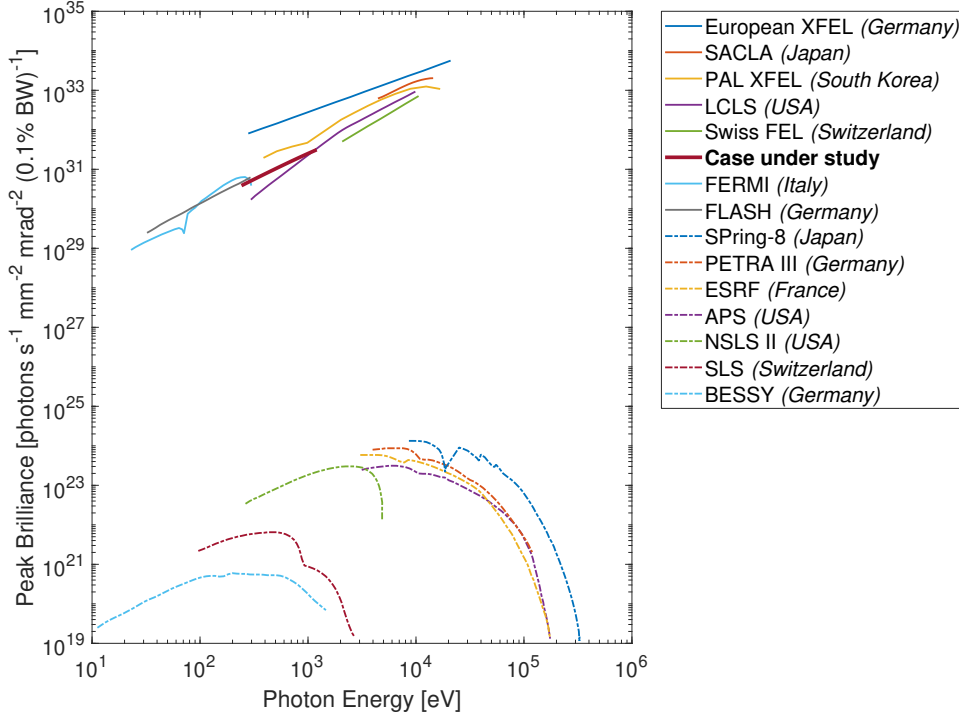


Figure 1: Peak brilliance as a function of photon energy for a selected set of light sources. Free-electron laser facilities are shown in solid lines, and synchrotron facilities are shown in dashed lines. This figure is adapted from Fig. 1 in Ref. [15]. The curve labelled “case under study” is made from analytical calculations using the electron parameters in Table 2 and an undulator period of 20 mm.

2 Theoretical background

2.1 General remarks

The FEL has two main components: (i) a beam of relativistic electrons and (ii) an undulator. In the undulator, the electron beam interacts with and amplifies the radiation that it emits. In this article, we consider the operation mode of self-amplified spontaneous emission (SASE) [16, 17], whereby the growth in radiation power starts from the shot noise in the electron beam.

The undulator is a magnetic device with a temporally static and spatially periodic magnetic field along its length. The magnetic field is specified by two parameters: (i) the *undulator period* λ_u and (ii) the *undulator parameter*

$$K = \frac{e\lambda_u B_0}{2\pi m_e c}, \quad (1)$$

where B_0 is the magnetic field amplitude, e is the absolute value of the electron charge, m_e is the electron rest mass and c is the speed of light.

On the axis of the undulator, the fundamental wavelength of the radiation is given by

$$\lambda = \frac{\lambda_u}{2\gamma^2} (1 + a_u^2), \quad (2)$$

where $a_u = K/\sqrt{2}$ for a planar undulator and $a_u = K$ for a helical undulator. The Lorentz factor γ denotes the electron energy in unit of the rest energy $m_e c^2$.

A figure of merit for an FEL is the *peak brilliance* (see Fig. 1), which is the number of photons emitted per unit time, per unit cross-sectional area, per unit solid angle, within a bandwidth

(BW) of 0.1% of the central wavelength. A related quantity is the *average brilliance*, which is the peak brilliance multiplied by the duration of the light pulse and the repetition rate.

The peak brilliance and other FEL properties can be calculated analytically from the one-dimensional (1D) and three-dimensional (3D) theories, which are recapitulated in the appendices.

2.2 Magnetic field strength deliverable by an undulator

For the purpose of developing a compact FEL, it is advantageous to minimize the saturation length and maximize the peak brilliance. In turn, these require optimizing the undulator specifications, namely λ_u and K .

According to Eq. (1), K scales linearly with the magnetic field strength B_0 . In general, B_0 can be expressed by the Halbach formula [18]

$$B_0(g, \lambda_u) = h_1 \exp \left[-h_2 \left(\frac{g}{\lambda_u} \right) + h_3 \left(\frac{g}{\lambda_u} \right)^2 \right]. \quad (3)$$

Here g is the gap height, i.e. the separation between the two opposite rows of magnetic poles in the undulator. B_0 has the unit of tesla, while both λ_u and g have the unit of millimetre. The coefficients h_1 , h_2 and h_3 have different values for different undulators types and for different materials. Table 1 shows four examples for the in-vacuum undulator (IVU) and the cryogenic permanent-magnet undulator (CPMU).

Table 1: Halbach coefficients for different undulator types

Type	Material	h_1	h_2	h_3	Source
IVU	SmCo	2.94	4.62	1.37	Ref. [19]
IVU	NdFeB	3.28	4.51	1.20	Ref. [19]
CPMU	NdFeB	3.341	3.606	0.300	Ref. [20]
CPMU	PrFeB	3.502	3.604	0.359	Ref. [20]

For the superconducting undulator (SCU), the scaling law for B_0 is different from Eq. (3). An alternative formulation was devised in Ref. [21] and summarized in Ref. [20] as follows:

$$B_0(g, \lambda_u) = (0.28052 + 0.05798\lambda_u - 9 \times 10^{-4}\lambda_u^2 + 5 \times 10^{-6}\lambda_u^3) \exp \left[-\pi \left(\frac{g}{\lambda_u} - 0.5 \right) \right]. \quad (4)$$

Here B_0 has the unit of tesla, while λ_u and g have the unit of millimetre. Note that Eq. (4) applies to NbTi superconducting wires at 80% of the critical current density. For NbSn superconducting wires, the expression is otherwise identical to Eq. (4), except that it needs to be multiplied by a factor of 1.3 [20].

In both Eqs. (3) and (4), B_0 can be increased by increasing λ_u or decreasing g . For any given λ_u , the largest achievable B_0 is limited by the smallest acceptable g , which is determined by the beam stay-clear (BSC). It then follows from Eq. (1) that

$$K_{\max}(\lambda_u) = \frac{e}{2\pi m_e c} \lambda_u B_0(g_{\min}, \lambda_u). \quad (5)$$

Using Eq. (5), we can calculate the maximum K deliverable as a function of λ_u for different undulator types and for different materials.

3 Results and discussions

3.1 Analytical calculations

Using the 3D FEL theory outlined in Appendix B, we perform analytical calculations for a case of the Soft X-Ray Laser (SXL) project [14] at the MAX IV Laboratory in Sweden.

The SXL is a planned FEL facility, which would utilize the electron beam from the existing linear accelerator at MAX IV. The target range for the radiation wavelength λ is 1–5 nm. Here we consider a case which uses (i) the SASE operation mode, (ii) variable-gap planar undulators and (iii) the electron parameter values shown in Table 2.

Table 2: Electron parameters in the case under study

Parameter	Symbol	Value
Electron energy	$\gamma m_e c^2$	3 GeV
Relative energy spread	σ_γ/γ	10^{-4}
Peak current	I_0	1.4 kA
Normalized emittance	ϵ_n	0.4 mm mrad
Average of beta function	β	5 m

To investigate the dependence of the FEL performance on the undulator specifications, we examine the four colourmaps in Fig. 2. Each colourmap shows the variation of a performance parameter over the K - λ_u plane, specifically in the region corresponding to the target wavelength range of $\lambda = 1$ –5 nm.

Given the undulator period λ_u , the desired wavelength λ can be obtained by adjusting the gap height g (and hence the undulator parameter K) to satisfy Eq. (2). Within Fig. 2(a), a larger λ_u yields a higher saturation power P_{sat} . Within Fig. 2(b), a smaller λ_u yields a smaller saturation length L_{sat} . Within Fig. 2(c), a smaller λ_u yields a longer coherence time τ_c . Within Fig. 2(d), a smaller λ_u yields a higher peak brilliance B .

For the purpose of developing a compact FEL, we want the largest B over the smallest L_{sat} . To this end, a useful figure of merit is the ratio B/L_{sat} , for which a colourmap is shown in Fig. 3. Within the domain of Fig. 3, the largest B/L_{sat} occurs at $\lambda_u = 15$ mm.

However, not all regions of the K - λ_u plane are accessible in practice. For any given λ_u , there is an upper limit for K given by $K_{\text{max}}(\lambda_u)$ in Eq. (5). The grey and purple curves in Fig. 3 show the function $K_{\text{max}}(\lambda_u)$ for six combinations of undulator types and materials. The stay-clear gap is assumed to be 3.0 mm for all six scenarios. This corresponds to a magnetic gap of $g = 4.8$ mm for the undulator type of SCU, and $g = 3.2$ mm for the other undulator types.

In each of the six scenarios, the accessible region of the K - λ_u plane is that below (and to the right of) the curve. Amongst the six scenarios, the undulator type of SCU with the material of NbSn has the largest K_{max} at any given λ_u (see Fig. 3). However, in order to cover the entire target wavelength range of $\lambda = 1$ –5 nm, the smallest possible choice for λ_u is 20 mm.

With $\lambda_u = 20$ mm, the peak brilliance B ranges from 3.9×10^{30} to 3.1×10^{31} photons $\text{s}^{-1} \text{mm}^{-2} \text{mrad}^{-2} (0.1\% \text{ BW})^{-1}$ in Fig. 2(d). This result is also shown in Fig. 1 by the curve labelled “case under study” to facilitate comparison with existing FEL facilities.

In Fig. 1, the SASE FELs reaching the photon energy range of the case under study are: FLASH, LCLS, PAL XFEL and European XFEL. Note that FERMI is seeded, and is not a SASE FEL. In terms of peak brilliance, the case under study is comparable to all the aforementioned SASE FELs, except the state-of-the-art European XFEL.

In terms of the undulator length, however, the case under study outperforms the existing FEL facilities significantly. In Fig. 2(b), with $\lambda_u = 20$ mm, the saturation length L_{sat} ranges from 7.7 to 12 m. This means that the total undulator length can be as short as 12 m in our case. Putting this into perspective, the total undulator length is 27 m for FLASH [22], 35 m for

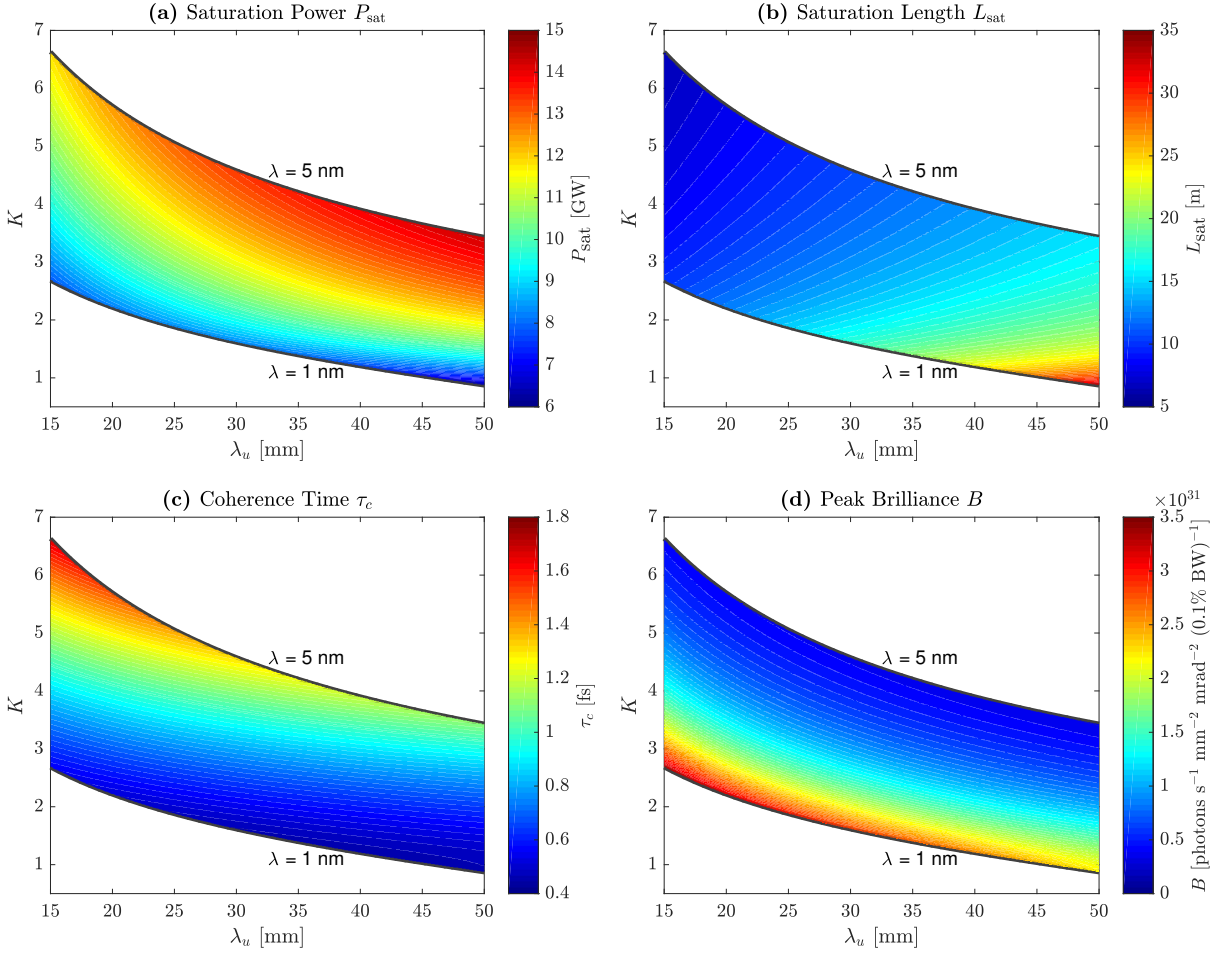


Figure 2: Colourmaps showing the variations of the four following parameters over the K - λ_u plane, in the region corresponding to the wavelength range of $\lambda = 1$ – 5 nm: (a) saturation power P_{sat} , (b) saturation length L_{sat} , (c) coherence time τ_c at saturation and (d) peak brilliance B at saturation.

the soft-x-ray undulator line of the PAL XFEL [23], 105 m for the SASE3 undulator line of the European XFEL [24], and 112 m for LCLS [25].

3.2 Numerical simulations

We supplement the analytical calculations with numerical simulations, using the 3D and time-dependent simulation code GENESIS [26].

In the simulations, the electron parameters remain the same as in Table 2. Meanwhile, we choose the operation point $\lambda_u = 15$ mm, $K = 2.68$ and $\lambda = 1$ nm, which corresponds to the largest B/L_{sat} in Fig. 3. This operation point is accessible by the undulator type of SCU with the material of NbSn.

The undulator line of a SASE FEL is usually segmented, with individual undulator modules separated by break sections. The purpose of the break sections is to provide space for the installation of focusing magnets, corrector magnets, phase shifters, diagnostics instruments etc.

In the simulations, each undulator module has a length of 2.7 m, and each break section has a length of 0.6 m. This is summarized in Table 3.

The focusing lattice is in a FODO configuration. The strengths of the quadrupole magnets are adjusted to deliver the average beta value specified in Table 2.

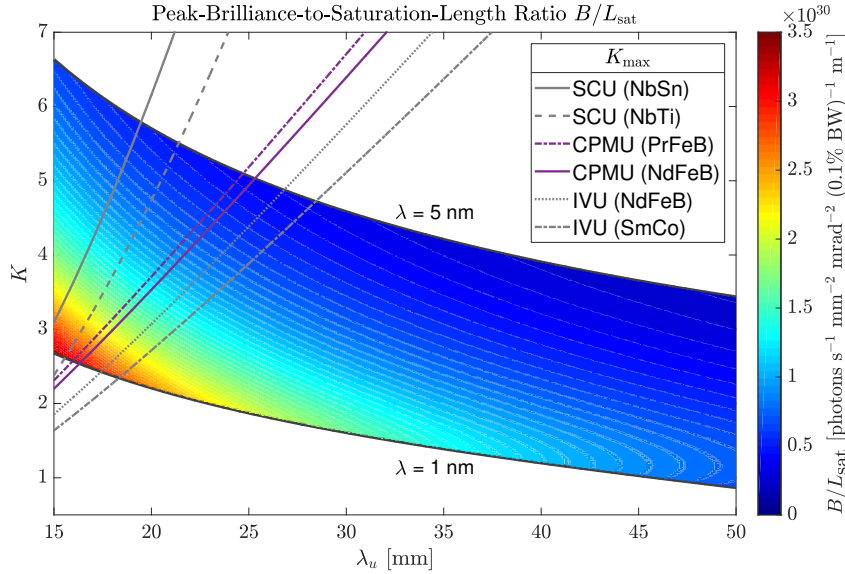


Figure 3: Colourmap showing the variation of the ratio B/L_{sat} over the K - λ_u plane, in the region corresponding to the wavelength range of $\lambda = 1$ – 5 nm. Here B is the peak brilliance at saturation and L_{sat} is the saturation length. The grey and purple curves show the maximum K deliverable as a function of λ_u for different undulator types and for different materials.

Table 3: Operation point used in the numerical simulations

Parameter	Symbol	Value
Radiation wavelength	λ	1 nm
Undulator period	λ_u	15 mm
Undulator parameter	K	2.68
Length of each undulator module	–	2.7 m
Length of each break section	–	0.6 m
RMS length of electron bunch	σ_z	9 μm

The SASE operation mode has a stochastic nature. We therefore simulate a total of 99 SASE shots, and examine the average behaviour. The results are shown in Fig. 4.

Fig. 4(a) shows the evolution of the peak brilliance along the undulator line. If we define the saturation point as the point of maximum peak brilliance, then saturation point occurs at $z = 15.9$ m with a peak brilliance of 3.7×10^{31} photons $\text{s}^{-1} \text{mm}^{-2} \text{mrad}^{-2}$ (0.1% BW). Excluding the break sections, the net undulator length required to reach the saturation point is 13.5 m.

Fig. 4(b) shows the power spectrum at the saturation point $z = 15.9$ m. Upon fitting the averaged spectrum to a Gaussian distribution, the rms bandwidth is found to be $\sigma_\lambda/\lambda = 1.1 \times 10^{-3}$.

3.3 Exploring other operation modes

So far, we have considered SASE, which is arguably the standard and the most reliable operation mode for x-ray FELs. However, SASE has a stochastic nature and can yield a noisy spectrum. In attempt to improve the spectral purity, one could consider various seeding options.

In the x-ray spectral region, no direct external seed is available, and one could consider self-seeding [27]. However, that would increase the required undulator length and inevitably make the FEL less compact. For the options of cascaded high-gain harmonic generation (HG HG) [28]

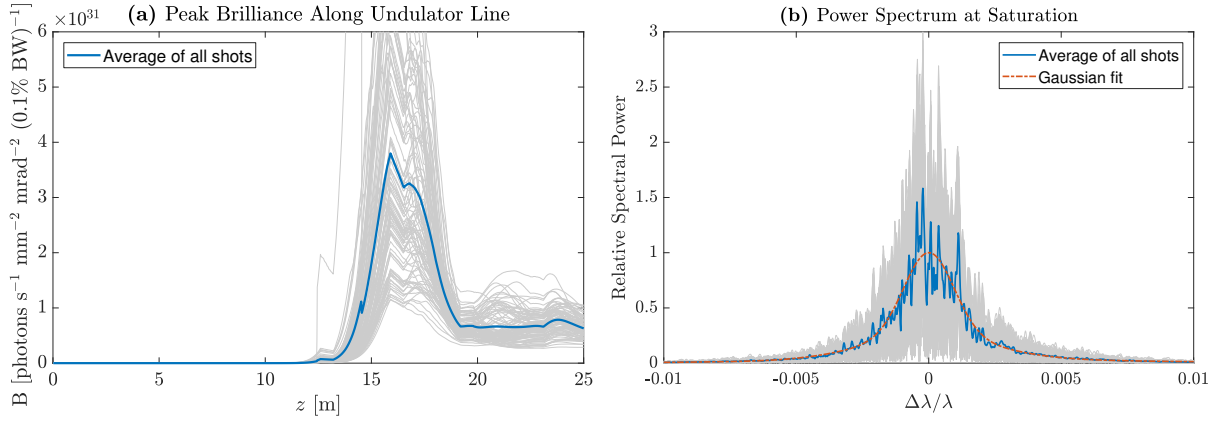


Figure 4: Simulation results: (a) peak brilliance B as a function of the distance z along the undulator line; (b) power spectrum at the saturation point $z = 15.9$ m, with the vertical axis showing the spectral power relative to the peak value of the Gaussian fit. Each grey curve corresponds to one SASE shot, and the blue curve shows the average of all the 99 shots.

and echo-enabled harmonic generation (EEHG) [29], the reduction in undulator length is expected to be very small and is outweighed by the demands for additional hardware (such as synchronized seed lasers and magnetic chicanes).

Another seeding option is harmonic-lasing self-seeding (HLSS) [30]. It provides an upgrade from the SASE configuration in terms of an improved peak brilliance and a shorter saturation length. The undulator line is divided into two sections of different K values, such that the h^{th} harmonic ($h > 1$) of the radiation produced in the first section serves as the seed at the fundamental wavelength for the second section. The harmonic lasing of the first section stays below saturation and the amplification proceeds to saturation in the second section. This way the reduced bandwidth of the harmonic, compared with the fundamental at the same wavelength, can be combined with the higher saturation power of the fundamental. Consequently an increased peak brilliance is obtained for which the enhancement factor over the corresponding SASE case is [30]

$$R = \frac{h\sqrt{L_u L_{\text{sat},h}}}{L_{\text{sat},1}}. \quad (6)$$

Here L_u is the length of the first undulator section; $L_{\text{sat},1}$ and $L_{\text{sat},h}$ are the saturation lengths of the fundamental and the harmonic, respectively. See further details in Appendix C.

Fig. 5 shows the enhancement factor, R , in the K - λ_u plane for the region corresponding to the output wavelengths of $\lambda = 1$ –5 nm. Here, we have assumed an equal length of the first (harmonic) and the second (fundamental) undulator sections, which corresponds to $L_u = 0.58 L_{\text{sat},h}$. Fig. 5 also shows the required K value limits for the fundamental (blue lines) and the harmonic (black lines) for the 1–5 nm output wavelengths. At $\lambda_u = 25$ mm, a K value of 9 is needed for the 3rd harmonic undulators which can be produced by the SCU (NbSn), as shown in Fig. 5. This undulator period provides an enhancement of the peak brilliance compared with SASE of $R = 1.64$ – 1.74 , for $\lambda = 1$ –5 nm.

The shorter saturation length of the harmonic lasing compared with the fundamental lasing at the same wavelength (see Appendix C) is advantageous for obtaining a compact FEL. We estimate the saturation length of the above HLSS system for $\lambda_u = 25$ mm as the sum of the fractional distribution of the saturation lengths of the first and second undulator section: $L_{\text{sat}} = 0.58 L_{\text{sat},h} + 0.42 L_{\text{sat},1}$. With $L_{\text{sat},h} = 10.3$ m and $L_{\text{sat},1} = 14.5$ m at $\lambda = 1$ nm, corresponding to the longest undulator system, we obtain $L_{\text{sat}} = 12.1$ m, which is similar to that obtained for the SASE system with $\lambda_u = 20$ mm. Hence, we conclude that an equally compact FEL can be obtained by a HLSS system with $\lambda_u = 25$ mm, as a SASE system with $\lambda_u = 20$ mm, but with a

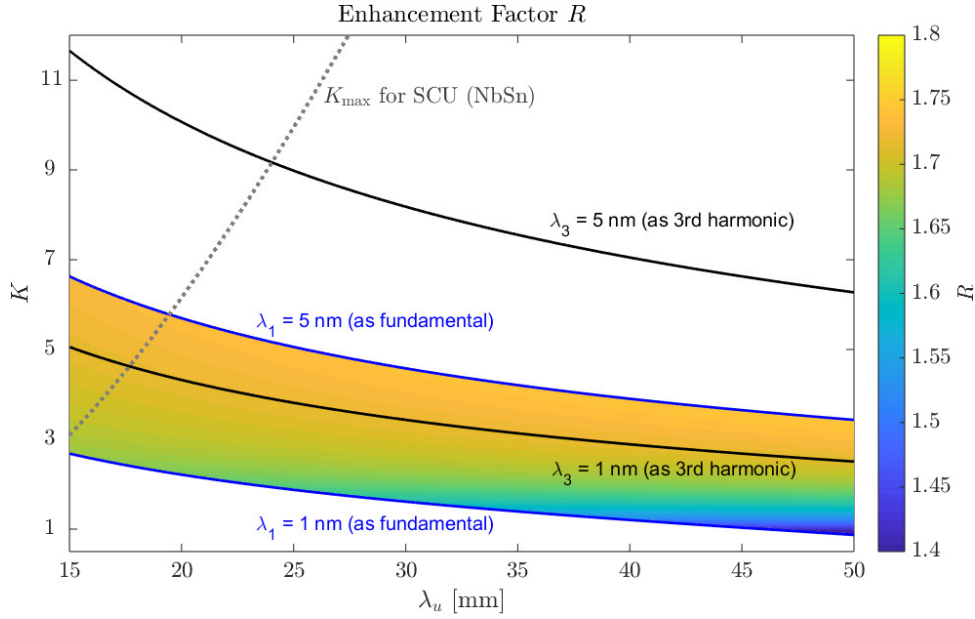


Figure 5: Colourmap for the enhancement factor R for the coherence time, and hence the peak brilliance, upon switching from SASE to HLSS. In this example of HLSS, the 3rd harmonic of the radiation produced in the first undulator section equals the fundamental wavelength for the second undulator section. The desired range of output wavelengths is 1–5 nm. The blue curves correspond to producing 1 and 5 nm as the fundamental wavelength in the second undulator section, while the black curves correspond to producing 1 and 5 nm as the 3rd harmonic in the first undulator section.

factor of 1.7 improved peak brilliance.

On a separate note, it is possible to enhance the peak brilliance of the FEL further by means of post-saturation tapering [31,32] or the phase jump method [33]. However, these techniques inevitably increase the total undulator length required, and offer limited benefit to the peak-brilliance-to-undulator-length ratio.

4 Conclusion

In this article, we have surveyed the recent progress on undulator technologies and studied analytically as well as numerically a case of a compact high-brilliance x-ray FEL.

For three undulator technologies: (i) in-vacuum, (ii) cryogenic and (iii) superconducting undulators, the analytical expressions for the peak magnetic field as a function of the undulator period and gap are presented. The Halbach coefficients for different undulator types and different magnetic materials are summarized in Table I. We deduce the possible undulator performance for a stay-clear gap of 3 mm that is compatible with FEL operation at low repetition rate. For peak undulator fields in the tesla range, the minimum undulator period is in the range of 15–20 mm depending on the undulator technology (see Fig. 3).

The maps of parameter space for the optimal FEL operation are calculated analytically and a numerical example using the GENESIS simulation code is presented for a selected set of parameters. The results strongly indicate that state-of-the-art magnet-based undulator technologies would allow the shortening of the total required undulator length by more than a *factor of two* while preserving (or even improving) the x-ray brilliance.

Furthermore, keeping the total undulator length fixed, the coherence and brilliance can be improved by operating in the HLSS mode. In our example, the first part of the undulator is tuned to the fundamental wavelength of 3 nm and the third harmonic is used to seed the

second part of the undulator tuned to the fundamental wavelength of 1 nm. The total required undulator length is 12 m, which is approximately the same as in the SASE mode, but the coherence time is improved by 70%.

Short-period undulators can be applied to upgrade the existing FEL facilities towards shorter wavelengths while keeping the undulator length unchanged. With the superconducting undulator technology, the total active undulator length required to bring the FEL lasing to saturation can be as short as 12 m at a lasing wavelength of $\lambda = 1$ nm. At $\lambda = 5$ nm, the required undulator length is around 8 m. For comparison, at the FLASH facility [22] in Germany, the FEL saturation at the same wavelength of 5 nm is reached within an active undulator length of around 20 m. Therefore, our study underpins the potential of making new x-ray FELs *more compact* than the existing ones, by taking advantage of the advancements in magnetic undulator technologies. Such high-brilliance x-ray FELs would offer new opportunities to all manners of user experiments and would increase the scientific output.

Funding

The European Union's Horizon 2020 Research and Innovation Programme (777431); Swedish Research Council (VR) (2016-04593), Royal Swedish Academy of Sciences (KVA) (PH2018-0037); Stockholm-Uppsala Centre for Free-Electron Laser Research (SUFEL).

Acknowledgments

The simulations were performed on resources provided by the Swedish National Infrastructure for Computing (SNIC) through the Uppsala Multidisciplinary Centre for Advanced Computational Science (UPPMAX) under project SNIC 2017/7-338. In addition, the authors thank Jim Clarke, Neil Thompson (Daresbury Laboratory, United Kingdom), Marie-Emmanuelle Couprie (SOLEIL, France) and Sverker Werin (MAX IV, Sweden) for the helpful discussions.

Appendix A 1D FEL theory

The 1D theory characterizes the FEL performance by the dimensionless *Pierce parameter*, which is defined as [17]

$$\rho = \frac{1}{2\gamma} \left(\frac{I_0}{I_A} \right)^{1/3} \left(\frac{\lambda_u K f_B}{2\pi\sigma_x} \right)^{2/3}. \quad (7)$$

Here, σ_x is the rms transverse radius of the electron beam, and I_0 is the peak current. Moreover, $I_A = 4\pi\epsilon_0 m_e c^3 / e$ is the Alfvén current, with ϵ_0 being the vacuum permittivity constant. For a planar undulator, the coupling factor

$$f_B = J_0 \left(\frac{K^2}{4 + 2K^2} \right) - J_1 \left(\frac{K^2}{4 + 2K^2} \right) \quad (8)$$

comprises two Bessel functions. For a helical undulator, $f_B = 1$.

In terms of the Pierce parameter ρ , the *gain length* can be written as [34]

$$L_{g,1D} = \frac{\lambda_u}{4\sqrt{3}\pi\rho}. \quad (9)$$

Meanwhile, the *saturation length* can be estimated as [34]

$$L_{\text{sat},1D} \approx \frac{\lambda_u}{\rho}, \quad (10)$$

and the *saturation power* can be estimated as [34]

$$P_{\text{sat,1D}} \approx \rho P_{\text{beam}}, \quad (11)$$

with $P_{\text{beam}} = \gamma m_e c^2 I_0 / e$ being the electron beam power. In Eq. (11), ρ can be interpreted as the *efficiency* of the FEL in converting the electron beam's power into radiation power. For x-ray FELs, ρ is typically on the order of 10^{-3} .

Appendix B 3D FEL theory

B.1 Saturation length and saturation power

The 1D FEL theory is an ideal case. It assumes that the electron beam has (i) zero emittance, (ii) zero energy spread, and (iii) a uniform transverse spatial distribution.

The Ming Xie parametrization [35] accounts for the deviations from the 1D theory, and formulates the gain length in the 3D theory as

$$L_g = [1 + \Lambda(\eta_d, \eta_\epsilon, \eta_\gamma)] L_{g,1D}, \quad (12)$$

with the correction factor

$$\begin{aligned} \Lambda(\eta_d, \eta_\epsilon, \eta_\gamma) = & a_1 \eta_d^{a_2} + a_3 \eta_\epsilon^{a_4} + a_5 \eta_\gamma^{a_6} + a_7 \eta_\epsilon^{a_8} \eta_\gamma^{a_9} + a_{10} \eta_d^{a_{11}} \eta_\gamma^{a_{12}} \\ & + a_{13} \eta_d^{a_{14}} \eta_\epsilon^{a_{15}} + a_{16} \eta_d^{a_{17}} \eta_\epsilon^{a_{18}} \eta_\gamma^{a_{19}}. \end{aligned} \quad (13)$$

The correction factor is a function of three variables:

$$\eta_d = \left(\frac{\lambda}{4\pi\sigma_x^2} \right) L_{g,1D} \quad (14)$$

measures the gain reduction due to diffraction,

$$\eta_\epsilon = \left(\frac{4\pi\epsilon}{\lambda} \right) \left(\frac{L_{g,1D}}{\bar{\beta}} \right) \quad (15)$$

measures the gain reduction due to the emittance ϵ , and

$$\eta_\gamma = \left(\frac{\sigma_\gamma}{\gamma} \right) \left(\frac{L_{g,1D}}{\lambda_u} \right). \quad (16)$$

measures the gain reduction due to the rms energy spread $\sigma_\gamma m_e c^2$.

Recall that the rms transverse radius of the electron beam is given by $\sigma_x = \sqrt{\bar{\beta}\epsilon}$, where $\bar{\beta}$ is the average of the beta function. Recall also that the emittance ϵ can be written in terms of the normalized emittance ϵ_n as $\epsilon = \epsilon_n / \gamma$.

The coefficients a_j ($j = 1, 2, \dots, 19$) are determined by fitting the numerical solution of the coupled Maxwell-Vlasov equations, and their values are listed in Table 4.

Table 4: Coefficients for the Ming Xie parametrization

$a_1 = 0.45$	$a_2 = 0.57$	$a_3 = 0.55$	$a_4 = 1.6$
$a_5 = 3$	$a_6 = 2$	$a_7 = 0.35$	$a_8 = 2.9$
$a_9 = 2.4$	$a_{10} = 51$	$a_{11} = 0.95$	$a_{12} = 3$
$a_{13} = 5.4$	$a_{14} = 0.7$	$a_{15} = 1.9$	$a_{16} = 1140$
$a_{17} = 2.2$	$a_{18} = 2.9$	$a_{19} = 3.2$	Source: [35]

By extension, the saturation power and saturation length in the 3D theory can be obtained from the following formulae: [35]

$$P_{\text{sat}} \approx 1.6\rho \left(\frac{L_{g,1D}}{L_g} \right)^2 P_{\text{beam}}, \quad (17)$$

$$L_{\text{sat}} = L_g \ln \left(\frac{P_{\text{sat}}}{\alpha P_0} \right). \quad (18)$$

Here $\alpha = 1/9$ is the scaling factor, and P_0 is the initial radiation power. For a SASE FEL, we have the effective shot noise power $P_0 \approx \rho^2 \gamma m_e c^3 / \lambda$.

B.2 Coherence properties

The coherence properties of a SASE FEL can be analysed in the approach of Saldin et al. [36]. The *coherence time* at saturation can be estimated as

$$\tau_c \approx \frac{1}{\bar{\rho}\omega} \sqrt{\frac{\pi \ln N_c}{18}}, \quad (19)$$

where $N_c = I/(e\bar{\rho}\omega)$ is the number of cooperating electrons, $\omega = 2\pi c/\lambda$ is the angular frequency of the radiation, $\bar{\rho} = \rho D^{1/3}$ is the equivalent of the Pierce parameter in the 3D theory, $D = 2\Gamma\sigma_x^2\omega/c$ is the diffraction parameter, and

$$\Gamma = \left(\frac{I_0}{I_A} \frac{8\pi^2 K^2 f_B^2}{\lambda\lambda_u\gamma^3} \right)^{1/2} \quad (20)$$

is the gain parameter.

The *degree of transverse coherence* at saturation is given by the fitting formula

$$\zeta \approx \frac{1.1\hat{\epsilon}^{1/4}}{1 + 0.15\hat{\epsilon}^{9/4}}, \quad (21)$$

where $\hat{\epsilon} = 2\pi\epsilon/\lambda$ is the scaled emittance. Note that the fit in Eq. (21) was done for $N_c = 4 \times 10^6$.

From the saturation power (17), we may compute the photon flux

$$\dot{N}_{\text{ph}} = \frac{dN_{\text{ph}}}{dt} = \frac{P_{\text{sat}}}{hc/\lambda}. \quad (22)$$

From here, we may compute the *degeneracy parameter*

$$\delta = \dot{N}_{\text{ph}}\tau_c\zeta \quad (23)$$

and hence the *peak brilliance*

$$B = \frac{4\sqrt{2}c\delta}{\lambda^3} \quad (24)$$

at saturation. It is customary to express the peak brilliance in the unit of photons $\text{s}^{-1} \text{mm}^{-2} \text{mrad}^{-2} (0.1\% \text{ bandwidth})^{-1}$. Note that Eq. (24) assumes a Gaussian-like radiation spectrum, whose rms bandwidth is given by $\sigma_\omega = \sqrt{\pi}/\tau_c$.

Appendix C Harmonic-lasing self-seeding

Consider two operation modes for the same output wavelength: self-amplified spontaneous emission (SASE) and harmonic-lasing self-seeding (HLSS). The latter enables an enhancement in coherence time (and hence peak brilliance) over the former. The enhancement factor R is given by Eq. (6), in which the quantity $L_{\text{sat},h}$ can be estimated as [37]

$$L_{\text{sat},h} \approx 0.6L_{g,h} \ln \left(hN_{\lambda_h} \frac{L_{g,h}}{\lambda_u} \right). \quad (25)$$

Here N_{λ_h} is the number of electrons per wavelength for harmonic number h and $L_{g,h}$ is the gain length of the harmonic.

The reduced gain length for the harmonic generation compared with the fundamental of the same wavelength can be clearly demonstrated for variable-gap undulators with a fixed undulator period. In this case the ratio between the gain length of the fundamental, $L_{g,1}$, and the harmonic, $L_{g,h}$, is:

$$\frac{L_{g,1}}{L_{g,h}} = \frac{h^{1/2} K_h A_{\text{J}h}(K_h)}{K A_{\text{J}1}(K)}, \quad (26)$$

where K_h and K are the undulator parameters of the first section (tuned to the harmonic) and second section (tuned to the fundamental), respectively. Also,

$$A_{\text{J}h}(K_h) = J_{(h-1)/2} \left(\frac{hK_h^2}{2(1+K_h^2)} \right) - J_{(h+1)/2} \left(\frac{hK_h^2}{2(1+K_h^2)} \right) \quad (27)$$

is the coupling factor for the harmonic h with J_n being Bessels functions. The ratio $L_{g,1}/L_{g,3} \approx 1.4$ for high K_3 values and increases rapidly for decreasing K_3 values approaching $\sqrt{2}$, where lasing at the fundamental becomes impossible. Generally $L_{\text{sat}} \approx 10L_g$.

References

- [1] F. Bencivenga, F. Capotondi, E. Principi, M. Kiskinova, and C. Masciovecchio, "Coherent and transient states studied with extreme ultraviolet and x-ray free electron lasers: present and future prospects," *Advances in Physics*, vol. 63, pp. 327–404, Apr 2015.
- [2] J. Ullrich, A. Rudenko, and R. Moshhammer, "Free-electron lasers: New avenues in molecular physics and photochemistry," *Annual Review of Physical Chemistry*, vol. 63, pp. 635–660, May 2012.
- [3] R. Neutze, G. Brändén, and G. F. Schertler, "Membrane protein structural biology using x-ray free electron lasers," *Current Opinion in Structural Biology*, vol. 33, pp. 115–125, Aug 2015.
- [4] H. N. Chapman, A. Barty, M. J. Bogan, S. Boutet, M. Frank, S. P. Hau-Riege, S. Marchesini, B. W. Woods, S. Bajt, W. H. Benner, R. A. London, E. Plönjes, M. Kuhlmann, R. Treusch, S. Düsterer, T. Tschentscher, J. R. Schneider, E. Spiller, T. Möller, C. Bostedt, M. Hoener, D. A. Shapiro, K. O. Hodgson, D. van der Spoel, F. Burmeister, M. Bergh, C. Caleman, G. Huldt, M. M. Seibert, F. R. N. C. Maia, R. W. Lee, A. Szöke, N. Timneanu, and J. Hajdu, "Femtosecond diffractive imaging with a soft-x-ray free-electron laser," *Nature Physics*, vol. 2, pp. 839–843, Nov 2006.
- [5] A. P. Mancuso, T. Gorniak, F. Staier, O. M. Yefanov, R. Barth, C. Christophis, B. Reime, J. Gulden, A. Singer, M. E. Pettit, T. Nisius, T. Wilhein, C. Gutt, G. Grübel, N. Guerassimova, R. Treusch, J. Feldhaus, S. Eisebitt, E. Weckert, M. Grunze, A. Rosenhahn, and I. A. Vartanyants, "Coherent imaging of biological samples with femtosecond pulses at the free-electron laser FLASH," *New Journal of Physics*, vol. 12, p. 035003, Mar 2010.

- [6] F. Capotondi, E. Pedersoli, N. Mahne, R. H. Menk, G. Passos, L. Raimondi, C. Svetina, G. Sandrin, M. Zangrando, M. Kiskinova, S. Bajt, M. Barthelmess, H. Fleckenstein, H. N. Chapman, J. Schulz, J. Bach, R. Frömter, S. Schleitner, L. Müller, C. Gutt, and G. Grübel, "Invited article: Coherent imaging using seeded free-electron laser pulses with variable polarization: First results and research opportunities," *Review of Scientific Instruments*, vol. 84, p. 051301, May 2013.
- [7] F. Capotondi, E. Pedersoli, F. Bencivenga, M. Manfredda, N. Mahne, L. Raimondi, C. Svetina, M. Zangrando, A. Demidovich, I. Nikolov, M. Danailov, C. Masciovecchio, and M. Kiskinova, "Multipurpose end-station for coherent diffraction imaging and scattering at FERMI@Elettra free-electron laser facility," *Journal of Synchrotron Radiation*, vol. 22, pp. 544–552, Apr 2015.
- [8] G. Smolentsev and V. Sundström, "Time-resolved x-ray absorption spectroscopy for the study of molecular systems relevant for artificial photosynthesis," *Coordination Chemistry Reviews*, vol. 304-305, pp. 117–132, Dec 2015.
- [9] S. Mukamel, D. Healion, Y. Zhang, and J. D. Biggs, "Multidimensional attosecond resonant x-ray spectroscopy of molecules: Lessons from the optical regime," *Annual Review of Physical Chemistry*, vol. 64, pp. 101–127, Apr 2013.
- [10] Z. Huang, "X-Ray FEL R&D: Brighter, better and cheaper," in *Proceedings of the 37th International Free-Electron Laser Conference, Daejeon, Korea*, pp. 7–9, JACoW, Geneva, Switzerland, Dec 2015.
- [11] "Compact Light Project Homepage." <http://www.compactlight.eu>.
- [12] J.-C. Huang, H. Kitamura, C.-K. Yang, C.-H. Chang, C.-H. Chang, and C.-S. Hwang, "Challenges of in-vacuum and cryogenic permanent magnet undulator technologies," *Physical Review Accelerators and Beams*, vol. 20, Jun 2017.
- [13] J. Bahrndt and E. Gluskin, "Cryogenic permanent magnet and superconducting undulators," *Nuclear Instruments and Methods in Physics Research Section A*, Apr 2018.
- [14] S. Werin, J. Andersen, S. Bonetti, F. Curbis, V. Goryashko, L. Isaksson, P. Johnsson, M. Kotur, M. Larsson, F. Lindau, E. Mansten, A. Nilsson, D. Olsson, P. Salén, H. Tarawneh, P. Tavares, S. Thorin, and O. Tjernberg, "The Soft X-Ray Laser project at MAX IV," in *Proceedings of the 8th International Particle Accelerator Conference, Copenhagen, Denmark*, pp. 2760–2762, JACoW, Geneva, Switzerland, May 2017.
- [15] E. Weckert, "The potential of future light sources to explore the structure and function of matter," *IUCr*, vol. 2, pp. 230–245, Feb 2015.
- [16] A. M. Kondratenko and E. L. Saldin, "Generating of coherent radiation by a relativistic electron beam in an undulator," *Particle Accelerators*, vol. 10, pp. 207–216, 1980.
- [17] R. Bonifacio, C. Pellegrini, and L. Narducci, "Collective instabilities and high-gain regime in a free electron laser," *Optics Communications*, vol. 50, pp. 373–378, Jul 1984.
- [18] K. Halbach, "Permanent magnet undulators," *Le Journal de Physique Colloques*, vol. 44, pp. C1–211–C1–216, Feb 1983.
- [19] R. Dejus, M. Jaski, and S. H. Kim, "On-axis brilliance and power of in-vacuum undulators for the advanced photon source," Tech. Rep. ANL/APS/LS-314, Argonne National Laboratory, USA, Nov 2009.

- [20] E. R. Moog, R. J. Dejus, and S. Sasaki, "Comparison of achievable magnetic fields with superconducting and cryogenic permanent magnet undulators – a comprehensive study of computed and measured values," Tech. Rep. ANL/APS/LS-348 137001, Argonne National Laboratory, USA, Jan 2017.
- [21] S. Kim, "A scaling law for the magnetic fields of superconducting undulators," *Nuclear Instruments and Methods in Physics Research Section A*, vol. 546, pp. 604–619, Jul 2005.
- [22] K. Honkavaara, "Status of the FLASH FEL user facility at DESY," in *Proceedings of the 38th International Free-Electron Laser Conference, Santa Fe, NM, USA, JACoW, Geneva, Switzerland*, Feb 2018.
- [23] I. Ko, H.-S. Kang, H. Heo, C. Kim, G. Kim, C.-K. Min, H. Yang, S. Baek, H.-J. Choi, G. Mun, B. Park, Y. Suh, D. Shin, J. Hu, J. Hong, S. Jung, S.-H. Kim, K. Kim, D. Na, S. Park, Y. Park, Y. Jung, S. Jeong, H. Lee, S. Lee, S. Lee, B. Oh, H. Suh, J.-H. Han, M. Kim, N.-S. Jung, Y.-C. Kim, M.-S. Lee, B.-H. Lee, C.-W. Sung, I.-S. Mok, J.-M. Yang, Y. Parc, W.-W. Lee, C.-S. Lee, H. Shin, J. Kim, Y. Kim, J. Lee, S.-Y. Park, J. Kim, J. Park, I. Eom, S. Rah, S. Kim, K. H. Nam, J. Park, J. Park, S. Kim, S. Kwon, R. An, S. Park, K. Kim, H. Hyun, S. Kim, S. Kim, C.-J. Yu, B.-S. Kim, T.-H. Kang, K.-W. Kim, S.-H. Kim, H.-S. Lee, H.-S. Lee, K.-H. Park, T.-Y. Koo, D.-E. Kim, and K. Lee, "Construction and commissioning of PAL-XFEL facility," *Applied Sciences*, vol. 7, p. 479, May 2017.
- [24] E. Schneidmiller and M. Yurkov, "Baseline parameters of the European XFEL," in *Proceedings of the 38th International Free-Electron Laser Conference, Santa Fe, NM, USA, JACoW, Geneva, Switzerland*, Feb 2018.
- [25] P. Emma, R. Akre, J. Arthur, R. Bionta, C. Bostedt, J. Bozek, A. Brachmann, P. Bucksbaum, R. Coffee, F.-J. Decker, Y. Ding, D. Dowell, S. Edstrom, A. Fisher, J. Frisch, S. Gilevich, J. Hastings, G. Hays, P. Hering, Z. Huang, R. Iverson, H. Loos, M. Messerschmidt, A. Miahnahri, S. Moeller, H.-D. Nuhn, G. Pile, D. Ratner, J. Rzepiela, D. Schultz, T. Smith, P. Stefan, H. Tompkins, J. Turner, J. Welch, W. White, J. Wu, G. Yocky, and J. Galayda, "First lasing and operation of an ångstrom-wavelength free-electron laser," *Nature Photonics*, vol. 4, pp. 641–647, Aug 2010.
- [26] S. Reiche, "GENESIS 1.3: a fully 3d time-dependent FEL simulation code," *Nuclear Instruments and Methods in Physics Research Section A*, vol. 429, pp. 243–248, Jun 1999.
- [27] J. Feldhaus, E. Saldin, J. Schneider, E. Schneidmiller, and M. Yurkov, "Possible application of x-ray optical elements for reducing the spectral bandwidth of an x-ray SASE FEL," *Optics Communications*, vol. 140, pp. 341–352, Aug 1997.
- [28] L.-H. Yu, "High-gain harmonic-generation free-electron laser," *Science*, vol. 289, pp. 932–934, Aug 2000.
- [29] G. Stupakov, "Using the beam-echo effect for generation of short-wavelength radiation," *Physical Review Letters*, vol. 102, Feb 2009.
- [30] E. A. Schneidmiller, B. Faatz, M. Kuhlmann, J. Rönsch-Schulenburg, S. Schreiber, M. Tischer, and M. V. Yurkov, "First operation of a harmonic lasing self-seeded free electron laser," *Physical Review Accelerators and Beams*, vol. 20, p. 020705, Feb 2017.
- [31] N. Kroll, P. Morton, and M. Rosenbluth, "Free-electron lasers with variable parameter wigglers," *IEEE Journal of Quantum Electronics*, vol. 17, pp. 1436–1468, Aug 1981.
- [32] A. Mak, F. Curbis, and S. Werin, "Model-based optimization of tapered free-electron lasers," *Physical Review Special Topics - Accelerators and Beams*, vol. 18, Apr 2015.

- [33] A. Mak, F. Curbis, and S. Werin, "Phase jump method for efficiency enhancement in free-electron lasers," *Physical Review Accelerators and Beams*, vol. 20, Jun 2017.
- [34] Z. Huang and K.-J. Kim, "Review of x-ray free-electron laser theory," *Physical Review Special Topics – Accelerators and Beams*, vol. 10, p. 034801, Mar 2007.
- [35] M. Xie, "Exact and variational solutions of 3D eigenmodes in high gain FELs," *Nuclear Instruments and Methods in Physics Research, Section A*, vol. 445, pp. 59–66, May 2000.
- [36] E. L. Saldin, E. A. Schneidmiller, and M. V. Yurkov, "Statistical and coherence properties of radiation from x-ray free-electron lasers," *New Journal of Physics*, vol. 12, p. 035010, Mar 2010.
- [37] E. A. Schneidmiller and M. V. Yurkov, "Harmonic lasing in x-ray free electron lasers," *Physical Review Special Topics - Accelerators and Beams*, vol. 15, Aug 2012.